Proposal of Roll Angle Control Method Using Positive and Negative Anti-dive Force for Electric Vehicle with Four In-wheel Motors

Naoya Ochi, Hiroshi Fujimoto and Yoichi Hori
The University of Tokyo
5-1-5, Kashiwanoha, Kashiwa, Chiba, 227-8561, Japan
Phone: +81-4-7136-3881, +81-4-7136-4131, +81-4-7136-3846
Fax:+81-4-7136-3881, +81-4-7136-4132, +81-4-7136-3847
Email: n.ochi@hflab.k.u-tokyo.ac.jp, fujimoto@k.u-tokyo.ac.jp, hori@k.u-tokyo.ac.jp

***Abstract*—Electric vehicles (EVs) have been gaining a lot of attention due to its environmental friendliness. EVs can be controlled precisely with the quick response of the motor. Moreover, using in-wheel motors, several types of motion controls can be performed. Therefore, such motion control of EVs have been intensely researched.**

This paper focuses on the control of roll angle which occurs during cornering. If this roll angle becomes large, steering response will be deteriorated, and also stability will decrease. Therefore, it is necessary to appropriately control the roll angle. In this paper, roll angle control method using positive and negative anti-dive force for EVs with four in-wheel motors has been proposed. Using positive and negative anti-dive force, the number of necessary actuators such as active suspensions can be reduced. The proposed method is also considering workload control of each wheel based on least square method. By estimating the roll moment disturbance using the roll moment observer, roll angle control has become a robust control system against disturbances. Thus, the proposed method allows improvement of vehicle's stability, safety and riding comfort during cornering. The effectiveness of the proposed method is verified by simulation and experimental results. Results of the roll angle control system without workload consideration and results of the case with workload consideration are also compared.

I. Introduction

A. Research background

Nowadays, the environmental problems as global warming, exhaustion of fossil fuels, and air pollution have become more critical. Eco-car such as hybrid vehicles (HEVs) and electric vehicles (EVs) can reduce the emission greenhouse gasses, in contrast with internal-combustion engine vehicles. Therefore, the automobiles called eco-car are greatly paid attentions, especially EVs which have superior environmental-friendly aspects. In addition, EVs which are driven by electric motors have four advantage points [1].

– Development of in-wheel motors enables individual control of each wheel.
– Continuous and smooth braking torque can be generated by regeneration.
– Generated torque can be measured precisely from motor current.
– Quick torque response is available by motor current control.

These advantages are usefull for vehicle motion control. Author's research group has studied the estimation of slip-ratio by using quick torque responses and control of vehicle motion with two in-wheel motors [3]. In addition, there is study such as driving force and lateral force distribution control system by the workload equalization control using independent steering system and four in-wheel motors[4].

Moreover, vehicle attitude control and load control with active suspension has been studied [5], [6]. However, in these methods, the number of actuators increases. On the other hand, using positive and negative anti-dive force of IWM EVs, attitude and load can be controled [7], [8].

Positive and negative anti-dive force is a force acting in the vertical direction by structure of the suspension, when the driving force is exerted on the wheel. IWM EVs can put out a large positive and negative anti-dive force compared to EVs with on-board motor. But [7], the positive and negative anti-dive force was not strictly considered. Alternatively in [8], control system was model-base control method and generates a command value by feedforward.

B. Research motivation

Roll motion occurs during cornering. If this roll angle becomes large, steering response is deteriorated, and stability is also reduced. Therefore, it is necessary to appropriately control the roll angle.

In this paper, roll angle control using positive and negative anti-dive force is proposed. This method uses four in-wheel motors. In the conventional method, there was no robustness against disturbance due to command value generated with a feed-forward system. On the other hand, the proposed method is built by the observer-based control system. In this way, robust control is possible even when there is a disturbance or parameter variation.

However, since the driving force is changing greatly when roll angle control is performed, there is a possibility that safety is lowered. Therefore, as a safety control, equalization

(a) FPEV2-Kanon

(b) In-wheel motor

Fig. 1. Experimental vehicle

TABLE I
PARAMETERS OF FPEV2–KANON

Weight (M)	880 [kg]
Wheelbase (l)	1.70 [m]
distance between the front axle and the center of gravity (l_f)	0.999 [m]
distance between the rear axle and the center of gravity (l_r)	0.701 [m]
Front wheel tread width (d_f)	1.30 [m]
Rear wheel tread width (d_r)	1.30 [m]
Front wheel inertia $(J_{\omega f})$	1.24 [kg/m^2]
Rear wheel inertia $(J_{\omega r})$	1.26 [kg/m^2]
Radius of the wheel (r)	0.302 [m]

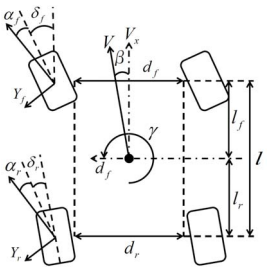

Fig. 2. Vehicle model

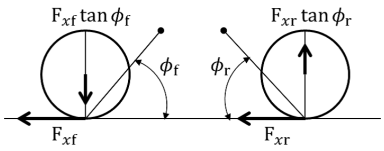

Fig. 3. Positive and Negative anti-dive force

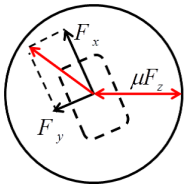

Fig. 4. Friction circle

control of tire workload based on the least squares method is incorporated in to the control system. In this way, it is possible to improve stability and safety during cornering.

II. EXPERIMENTAL VEHICLE

An original experimental EV "FPEV2-Kanon" that is developed in the author's laboratory, is used for performance verification. In this section, the characteristics of the experimental vehicle are explained. In-wheel motors which are outer-roter type, are installed in each wheel. Since this motor is the direct drive system, the reaction force from the road is directly transferred to the motor side without gear reduction and backlash. The maximum torque of front motors is $\pm$500 Nm, and the maximum torque of rear motors is $\pm$340 Nm. It is possible to generate yaw-moment using difference of driving force between left and right in-wheel motor. The steering mechanism adopts active front and rear steering system, using two 250W DC motors for electric power steering (EPS). Moreover, in order to switch Steer-by-Wire (SbW) and EPS, the steering wheel shaft has a removable structure. The features of experimental vehicle mainly utilized in this study are four in-wheel motors and the front active steering.

Fig. 1 (a) shows FPEV2-Kanon, Fig. 1 (b) shows rear in-wheel motor, and Table. I shows experimental vehicle's specification.

III. VEHICLE MODELING

A. Motion dynamics of the vehicle

In this section, it is explained about equations of motion of the vehicle which has independent steering system and four in-wheel motors [10]. Fig. 2 shows the vehicle model. The wheel dynamics is expressed as follows:

$$J_{\omega_i}\dot{\omega}_i = T_i - rF_{xi} \tag{1}$$

where J_{ω_i} is the wheel inertia, T_i is the motor torque, F_{xi} is the driving force, r is the wheel radius, and subscription i is substituted by fl, fr, rl, rr for front left, front right, rear left, and rear right, respectively. In addition, the equation for longitudinal motion, lateral motion, roll motion and yaw motion are represented by

$$\begin{aligned}
F_x &= F_{xfl} + F_{xfr} + F_{xrl} + F_{xrr} && (2)\\
F_y &\simeq M(\dot{\beta}+\gamma) = F_{yfl} + F_{yfr} + F_{yrl} + F_{yrr} && (3)\\
M_x &= \frac{d_f}{2}(-u_{zfl} + u_{zfr}) + \frac{d_r}{2}(u_{zrl} - u_{zrr})\\
&= G_{fl}F_{xfl} + G_{fr}F_{xfr} + G_{rl}F_{xrl} + G_{rr}F_{xrr} && (4)\\
M_{xall} &= Mh_s a_y + M_x && (5)\\
M_y &= -l_f u_{zfl} - l_f u_{zfr} + l_r u_{zrl} + l_r u_{zrr}\\
&= H_{fl}F_{xfl} + H_{fr}F_{xfr} + H_{rl}F_{xrl} + H_{rr}F_{xrr} && (6)\\
M_{yall} &= Mh_g a_x + M_y && (7)\\
M_z &= \frac{d_f}{2}(-F_{xfl} + F_{xfr}) + \frac{d_r}{2}(-F_{xrl} + F_{xrr}) && (8)\\
M_{zall} &\simeq F_{yfl}l_f + F_{yfr}l_f + F_{yrl}l_r + F_{yrr}l_r + M_z && (9)
\end{aligned}$$

where F_x is the total driving force of the vehicle, F_y is the lateral force, M_x is the roll moment by positive and negative anti-dive force, M_{xall} is the total roll moment of the vehicle, M_y is the pitch moment by positive and negative anti-dive force, M_{yall} is the total pitch moment of the vehicle, M_z is the yaw moment by difference driving force, M_{zall} is the total yaw moment of the vehicle, F_{xfl}, F_{xfr}, F_{xrl}, F_{xrr} are the driving force of each wheel, F_{yfl}, F_{yfr}, F_{yrl}, F_{yrr} are the lateral force of each wheel, M is the vehicle mass, β is the sideslip angle of the vehicle's center of gravity, γ is the angular velocity about the axis of rotation of the vehicle's center of gravity, h_s is the distance between the vehicle's center of rotation and center of gravity, a_y is the lateral acceleration, d_f and d_r are the tread width of the front and rear wheels and u_{zfl}, u_{zfr},

u_{zrl}, u_{zrr} are the positive and negative anti-dive force of each wheel.

Next, a description will be given for the positive and negative anti-dive force by each driving force. Fig. 3 shows the positive and negative anti-dive force by each driving force. Positive and negative anti-dive force is determined from the angle to the horizontal plane and the line connecting the instantaneous center of rotation of the suspension from the ground point. In this case, negative anti-dive force acts on the front wheels and positive anti-dive force acts on the rear wheels. The equation for positive and negative anti-dive force of the each wheel is represented by

$$u_{zfl} = -F_{xfl}\tan\phi_f \quad (10)$$
$$u_{zfr} = -F_{xfr}\tan\phi_f \quad (11)$$
$$u_{zrl} = F_{xrl}\tan\phi_r \quad (12)$$
$$u_{zrr} = F_{xrr}\tan\phi_r. \quad (13)$$

In addition, the vertical load of each wheel is expressed as follows:

$$F_{zfl} = \frac{1}{2}N_f - \frac{1}{2}a_x M\frac{h_g}{l_f+l_r} - \rho_f a_y M\frac{h_s}{d_f} - u_{zfl} \quad (14)$$
$$F_{zfr} = \frac{1}{2}N_f - \frac{1}{2}a_x M\frac{h_g}{l_f+l_r} + \rho_f a_y M\frac{h_s}{d_f} - u_{zfr} \quad (15)$$
$$F_{zrl} = \frac{1}{2}N_r + \frac{1}{2}a_x M\frac{h_g}{l_f+l_r} - \rho_r a_y M\frac{h_s}{d_r} - u_{zrl} \quad (16)$$
$$F_{zrr} = \frac{1}{2}N_r + \frac{1}{2}a_x M\frac{h_g}{l_f+l_r} + \rho_r a_y M\frac{h_s}{d_r} - u_{zrr} \quad (17)$$

where ϕ is the instantaneous center of rotation angle, N_f and N_f are the static load of the front and rear wheels, a_x is the longitudinal acceleration, h_g is the height of the vehicle's center of gravity, h_s is the distance between the vehicle's center of gravity and the vehicle's roll center, l_f and l_r are the distance from the vehicle's center of gravity to the front and rear wheel shaft and ρ_f and ρ_r are the front and rear roll stiffness distribution ratio.

There is also a relation like the friction circle as shown in Fig. 4 between the driving force F_x, the lateral force F_y and the vertical load F_z acting on each wheel. This relationship must always satisfy the following equation,

$$\sqrt{F_x^2 + F_y^2} \le \mu F_z \quad (18)$$

where μ is the friction coefficient of the road surface.

B. Equations of roll motion

Equation of motion of the roll will be as follows from the balance of roll moment by the positive and negative anti-dive force and roll moment due to rotational motion around the x-axis.

$$M_{xall} = \left(I_r s^2 + C_r s + K_r\right)\theta_r \quad (19)$$

where I_r is the moment of inertia about the roll axis of the vehicle body, C_r is the coefficient of the suspension damper and K_r is the spring constant of the suspension.

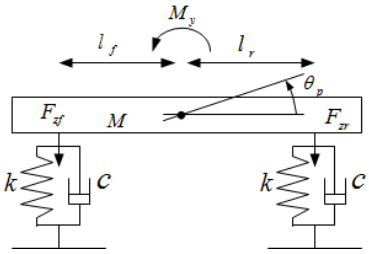

Fig. 5. Half car model

If the effect of gravity on the roll of the vehicle is negligible, the transfer function from roll moment M_{xall} to roll angle θ_r can be expressed as follows:

$$\theta_r = \frac{1}{I_r s^2 + C_r s + K_r}M_{xall} = \frac{1}{I_r s^2 + C_r s + K_r}\left(Mh_s a_y + M_x\right). \quad (20)$$

Parameters of the experimental vehicle in (20) are unknown. Therefore identification test is done. As a result,the value of each parameter is as follows: $I_r = 1.1 \times 10^2$ kgm^2, $C_r = 4.7 \times 10^3$ N/(m/s), $K_r = 2.1 \times 10^4$ N/m.

C. Equations of pitch motion

Since pitch motion varies by the attitude of the vehicle body, pitch motion can be approximated by a model that considers only the vehicle's center of gravity. Also, it is possible to use a two-wheeled model (half car model) because pitch motion is longitudinal movement. Fig. 5 shows the half car model. Pitch motion can be considered similar to roll motion. Equation of pitch motion can be expressed as follows:

$$\theta_p = \frac{1}{I_p s^2 + C_p s + K_p}M_{yall} = \frac{1}{I_p s^2 + C_p s + K_p}\left(Mh_g a_x + M_y\right). \quad (21)$$

Parameters of the experimental vehicle in (21) are unknown. Therefore identification test is done. As a result, the value of each parameter is as follows $I_p = 6.2 \times 10^2$ kgm^2, $C_p = 4.7 \times 10^3$ N/(m/s), $K_p = 8.9 \times 10^4$ N/m.

IV. Control System Design

Fig. 6 shows a block diagram of the proposed roll angle control system. This control system is composed of a speed control system and the roll angle control system. Moreover, roll angle control system is built by the observer-based control system.

In Fig. 6, z_{ij} is the length of each suspension, and roll angle θ_r is estimated from z_{ij}.

A. DFO (Driving Force Obsever)

Fig. 7 shows a block diagram of the Driving Force Obsever. Driving force obsever is a method to estimate the actually generated driving force F_{xi}. In (1), ω_i and T_i are measurable. Therefore, F_{xi} can be estimated.

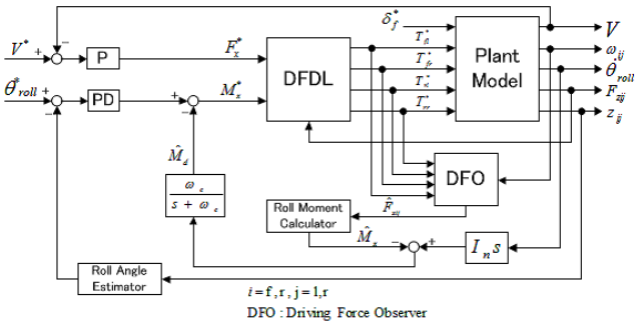

Fig. 6. Block diagram of control system

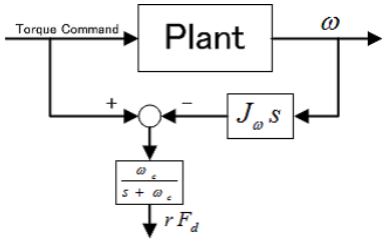

Fig. 7. Block diagram of DFO

B. RMO (Roll Moment Obsever)

Fig. 8 shows a block diagram of the Roll Moment Observer. When considering the disturbance, (20) can be expressed as (22):

$$(I_r s^2 + C_r s + K_r)\theta_r = Mh_s a_y + M_x + M_{xd} \tag{22}$$

where M_{xd} is the roll-moment disturbance. In this case, disturbance observer is constructed as shown in Fig. 8. Considering $M_{xad} = Mh_s a_y - C_r\dot{\theta} - K_r\theta + M_{xd}$ as the total disturbance, equation (23) can be nominalized as follows:

$$I_r\dot{\theta}_r \quad = \quad M_{xad} + M_x. \tag{23}$$

Here, using F_x which is estimated from the driving force observer, M_x is calculated from the relation in (4) at Roll Moment Calculator block in Fig. 8.

C. DFDL (Driving Force Distribution Law)

1) Roll angle control with workload consideration (Proposed method): The driving force of each wheel is generated by DFDL (Driving Force Distribution Law) in Fig. 6 to satisfy the condition expressed in (2) for command value from roll angle control system and in (5) for command value from the speed control system. Following is the calculation performed in DFDL. (24) shows equations of motion of the driving force and roll moment by positive and negative anti-dive force.

$$\begin{bmatrix} 1 & 1 & 1 & 1 \\ G_{fl} & G_{fr} & G_{rl} & G_{rr} \end{bmatrix} \begin{bmatrix} F_{xfl} \\ F_{xfr} \\ F_{xrl} \\ F_{xrr} \end{bmatrix} = \begin{bmatrix} F_x^* \\ M_x^* \end{bmatrix} \tag{24}$$

Here, the coefficient matrix on the left-hand side of (24) is defined as $\mathbf{A}$, column vector of the driving force of each wheel

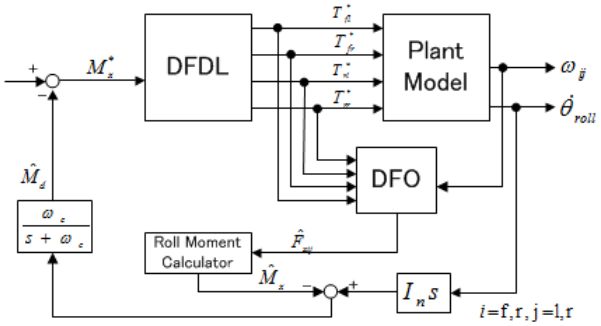

Fig. 8. Block diagram of RMO

$[F_{xfl}\ F_{xfr}\ F_{xrl}\ F_{xrr}]^T$ is defined as $\mathbf{x}$ and column vector on the left-hand side $[F_x^*\ M_x^*]^T$ is defined as $\mathbf{b}$. At this time, tire workload is defined as usage rate of friction circle by resultant force vector generated by each wheel as follows:

$$\eta_{ij} \quad = \quad \frac{\sqrt{F_{xij}^2 + F_{yij}^2}}{\mu_{\max} F_{zij}} \simeq \frac{\sqrt{F_{xij}^2 + F_{yi}^2}}{\mu_{\max} F_{zij}} \tag{25}$$

where subscription i is replaced by f, r as front and rear, and subscription j is replaced by l, r as left and right. Maximum coefficient of friction of each wheel μ_{max} is assumed to be equal, and the evaluation function is defined as the sum of the squares of the product of each wheel's workload η_{ij} and μ_{max}. Weighted least squares solution of (24) which minimizes J is defined as x_{opt} and weighting matrix is defined as W. Equations used in this relation are as follows:

$$\begin{aligned} J &= \sum_{i=f,r}\sum_{j=l,r} (\mu_{\max}\eta_{i,j})^2 = \sum_{i=f,r}\sum_{j=l,r} \frac{F_{xij}^2 + F_{yi}^2}{F_{zij}^2} \\ &= \frac{F_{xfl}^2}{F_{zfl}^2} + \frac{F_{xfr}^2}{F_{zfr}^2} + \frac{F_{xrl}^2}{F_{zrl}^2} + \frac{F_{xr}^2}{F_{zrr}^2} + K \\ &= x^T W x + K \quad (K = const) \qquad (26) \\ x_{opt} &= W^{-1}A^T(AW^{-1}A^T)^{-1}b \qquad (27) \\ W &= \mathrm{diag}\left(\frac{1}{F_{zfl}^2}, \frac{1}{F_{zfr}^2}, \frac{1}{F_{zrl}^2}, \frac{1}{F_{zrr}^2}\right). \qquad (28) \end{aligned}$$

In addition, the calculated driving force is input as the value of the motor torque command of each wheel using the relationship $T = rF_x$.

In the following section, this roll control system with workload consideration will be refered to as proposed method.

2) Roll angle control without workload consideration (Conventional method): To evaluate the performance of the proposed roll angle control considering workload, the roll control system without workload consideration is also examined.

In roll control system without workload consideration, driving force for each wheel is generated in DFDL block in Fig. 6. However, in additional to the longitudinal motion and roll motion, pitch motion and yaw motion are are considered instead of workload.

Summarizing (2), (4), (6), (8), system equation can be expressed as follows:

$$\begin{bmatrix} 1 & 1 & 1 & 1 \\ G_{fl} & G_{fr} & G_{rl} & G_{rr} \\ H_{fl} & H_{fr} & H_{rl} & H_{rr} \\ -\frac{d_f}{2} & -\frac{d_f}{2} & \frac{d_r}{2} & \frac{d_r}{2} \end{bmatrix} \begin{bmatrix} F_{xfl} \\ F_{xfr} \\ F_{xrl} \\ F_{xrr} \end{bmatrix} = \begin{bmatrix} F_x^* \\ M_x^* \\ M_y^* \\ M_z^* \end{bmatrix} \quad (29)$$

At this time, driving force for each wheel is generated using the inverse matrix of the coefficient matrix on the left side of (29), in a way that will not generate pitch and yaw motion ($M_y = 0, M_z = 0$).

In the following section, this roll control system without workload consideration will be refered to as conventional method.

V. Simulation

In this section, simulation is conducted for cornering with constant velocity and constant radius. The simulation results of conventional method and proposed method are compared. A vehicle speed control system is built to perform a comparison of the results of conventional method and proposed method at a constant speed. This vehicle speed control system uses a proportional controller. Pole placement method is carried out using plant considering the vehicle mass, based on the following equation,

$$V = \frac{1}{Ms} F_x. \quad (30)$$

Pole of speed control system is decided to be $w_v = -2\ \mathrm{rad/s}$.

According to organoleptic evaluation in [6], for lateral acceleration of $5\ \mathrm{m/s^2}$, the driver's comfort level is at best when roll angle is $0.017\ \mathrm{rad}$. However, verifying the effectiveness of the proposed method is the purpose of this paper. Therefore, roll angle command value was set to $0.022\ \mathrm{rad}$ reducing the roll angle from $0.027\ \mathrm{rad}$ when there is no roll angle control.

PD controller is selected for this system, and pole w_{roll} is decided to be $-20\ \mathrm{rad/s}$ by pole placement method applying to (20).

In order to verify the effectiveness of the proposed control system, simulations cornering motion is carried out in the road environment assuming the same condition as the actual experiment. Speed is $V = 15\ \mathrm{km/h}$ and cornering radius is $R = 10\ \mathrm{m}$. Fig. 9 and Fig. 10 show the simulation results.

The velocity properly follows the command value in each method as shown in Fig. 9 (a) and Fig. 10 (a). The roll angle also properly follows the command value in each method as shown in Fig. 9 (b) and Fig. 10 (b). However, the maximum workload of proposed method has been reduced compared to the conventional method as shown in Fig. 9 (c) and Fig. 10 (c). In addition, values of workload in the result of proposed method are smaller than those of conventional method overall, and workload of each wheel has been equalized. Regarding the driving force of each wheel in this case, the maximum value of the driving force has decreased, and each motor did not output excessive driving force as shown in Fig. 9 (d) and Fig. 10 (d).

Moreover, the pitch moment M_y and the yaw moment M_z due to the difference in the driving force are generated according to (6) and (8) in the proposed method. However, the effects are negligible, because the pitch moment due to distributed driving force is sufficiently small, and the yaw moment due to the difference in the driving force is sufficiently small compared to the yaw moment due to lateral force.

VI. Experiment

Experiments are performed for conventional method and proposed method under the same conditions as simulations. Using the experimental vehicle described in Section 2, experiments were carried out at the university campus test site. A potentiometer is attached to each suspension arm for measuring roll angle and wheel load. Fig. 11 and Fig. 12 show the experimental results. The vehicle speed is shown in Fig. 11(a) and Fig. 12(a). In these figure, both conventional method and proposed method followed command value, and have been driven at a constant speed. Next, the roll angle are shown in Fig. 11(b) and Fig. 12(b), and the workload are shown in Fig. 11(c) and Fig. 12(c). The roll angle is reduced with the same manner in conventional method and proposed method, and the output roll angle is following the command value. However, the maximum value of the workload in the proposed method is smaller compared with conventional method, and the workload has decreased overall, which is consistent with simulation. In addition, the maximum value of the driving force in proposed method has been reduced as unnecessary driving force is not generated.

VII. Conclusion

In this paper, we consider the roll angle control system with equalized workload control in electric vehicle equipped with four-in-wheel motors. It was confirmed that the proposed roll angle control system with the workload control (proposed method) is able to reduce the workload from control system without the workload control (conventional method) by simulation and experiment. The proposed method can be considered a safer roll angle control than conventional method.

In the future, cooperative control of roll, pitch and yaw motion will be considered. Moreover, the effectiveness of the proposed method will be verified in the new experimental vehicle which is currently in production. This new experimental vehicle can produce greater positive and negative anti-dive force with even smaller driving force.

References

[1] Y. Hori: "Future vehicle driven by electricity and control research on four-wheel-motored "UOT Electric March II"", IEEE Trans. on Industrial Electronics, Vol. 51, No. 5, pp. 954-962, 2004

[2] Toru Suzuki, Hiroshi Fujimoto: "Slip Ratio Estimation and Regenerative Brake Control without Detection of Vehicle Velocity and Acceleration for Electric Vehicle at Urgent Brake-turning", in Proceedings of The 11th International Workshop on Advanced Motion Control (AMC'10), pp.273-278, Niigata 2010

[3] D. Yin, Y. Hori: "A new approach to traction controlof EV based on maximum effective torque estimation", Proceedings of the 34th Annual Conference of the IEEE Industrial Electronics Society, IECON 2008, pp.2764-2769, 2008

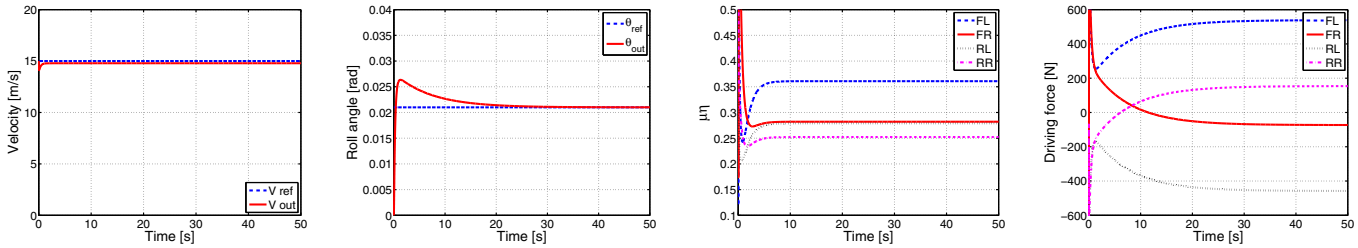

(a) Velocity (b) Roll angle (c) Tire workload (d) Driving force

Fig. 9. Simulation results (conventional method)

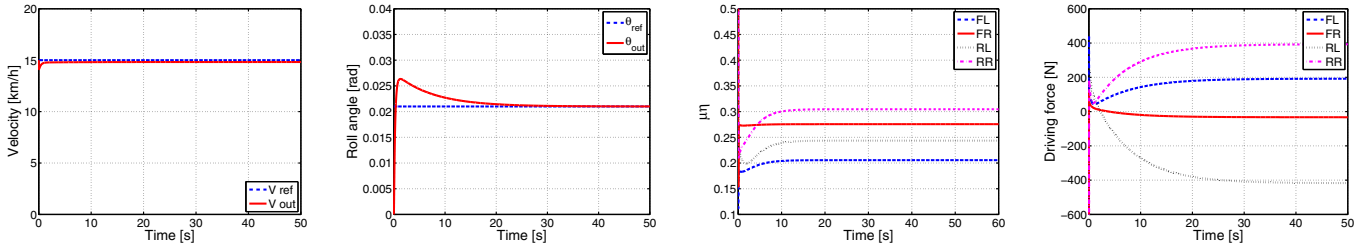

(a) Velocity (b) Roll angle (c) Tire workload (d) Driving force

Fig. 10. Simulation results (proposed method)

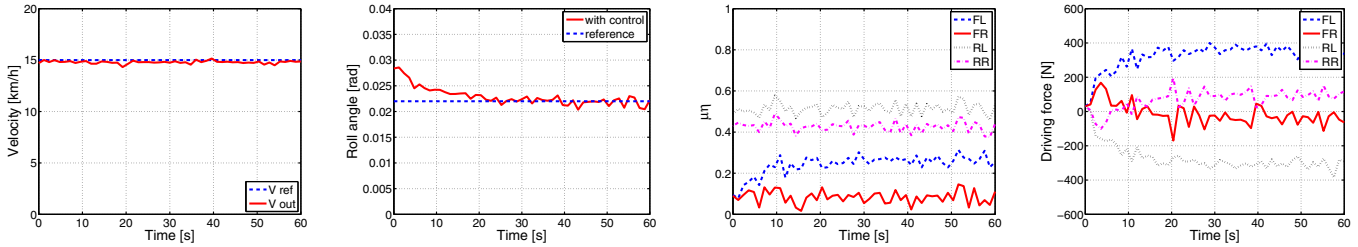

(a) Velocity (b) Roll angle (c) Tire workload (d) Driving force

Fig. 11. Experimental results (conventional method)

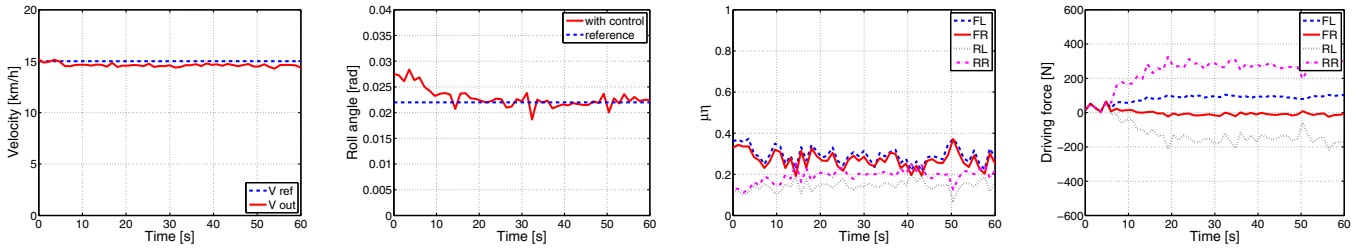

(a) Velocity (b) Roll angle (c) Tire workload (d) Driving force

Fig. 12. Experimental results (proposed method)

[4] Naoki Ando, Hiroshi Fujimoto: "Yaw-rate Control for Electric Vehicle with Active Front/Rear Steering and Driving/Braking Force Distribution of Rear Wheels", in Proceedings of The 11th International Workshop on Advanced Motion Control (AMC'10), pp. 273-278, Niigata 2010

[5] Y. Hanamura, K. Fujita, Y. Araki, M. Oya, H. Harada: "Control of Vehicle Maneuverability and Stability of 4 Wheeled Vehicle by Active Suspension Control with Additional Vertical Load Control", The Japan Society of Mechanical Engineers. C, No.98-0904, pp. 236-243, 1998 (in Japanese)

[6] S. Buma, H. Satou, T. Yonekawa, T. Ohnuma, K. Hattori, M. Sugihara: "Synthesis and Development of the Avtive Control Suspension", Transactions of the Japan Society of Mechanical Engineers. C, vol. 157, No. 534, pp. 257-263, 1991 (in Japanese)

[7] S. Sato, H. fujimoto: "Proposal of pitching Control for Electric Vehicle with In-Wheel Motor", IEE of Japan Technical Meeting Recoard, IIC–07–81, pp. 65-70, 2007 (in Japanese)

[8] E. Katsuyama: "Decoupled 3D Moment Control by In-Wheel Motor", JSAE 2011 Annual Congress(Spring), No.3-11, pp. 1-6, 2011 (in Japanese)

[9] N. Ando, H. Fujimoto: "Distribution and Control Methods of Driving/Braking Force and Lateral Force for Electric Vehicle with Lateral-force Sensors and In-wheel Motors in All-wheels and Active Front/Rear Steering", IEE of Japan Technical Meeting Recoard, IIC-10-102, pp. 29-34, 2010 (in Japanese)

[10] Masato Abe: "Vehicle Handling Dynamics", Butterworth-Heinemann (2009)